

## Wideband polarized radio emission from the newly revived magnetar XTE J1810–197

SHI DAI,<sup>1</sup> MARCUS E. LOWER,<sup>2,1</sup> MATTHEW BAILES,<sup>2,3</sup> FERNANDO CAMILO,<sup>4</sup> JULES P. HALPERN,<sup>5</sup> SIMON JOHNSTON,<sup>1</sup>  
MATTHEW KERR,<sup>6</sup> JOHN REYNOLDS,<sup>1</sup> JOHN SARKISSIAN,<sup>7</sup> AND PAUL SCHOLZ<sup>8</sup>

<sup>1</sup>*CSIRO Astronomy and Space Science, Australia Telescope National Facility, Epping, NSW 1710, Australia*

<sup>2</sup>*Centre for Astrophysics and Supercomputing, Swinburne University of Technology, PO Box 218, Hawthorn, VIC 3122, Australia*

<sup>3</sup>*OzGrav: The ARC Centre of Excellence for Gravitational-wave Discovery, Hawthorn VIC 3122, Australia*

<sup>4</sup>*South African Radio Astronomy Observatory, Observatory 7925, South Africa*

<sup>5</sup>*Columbia Astrophysics Laboratory, Columbia University, New York, NY 10027, USA*

<sup>6</sup>*Space Science Division, Naval Research Laboratory, Washington, DC 20375-5352, USA*

<sup>7</sup>*CSIRO Astronomy and Space Science, Parkes Observatory, PO Box 276, Parkes NSW 2870, Australia*

<sup>8</sup>*National Research Council of Canada, Herzberg Astronomy and Astrophysics, Dominion Radio Astrophysical Observatory, Penticton, BC V2A 6J9, Canada*

### ABSTRACT

The anomalous X-ray pulsar XTE J1810–197 was the first magnetar found to emit pulsed radio emission. After spending almost a decade in a quiescent, radio-silent state, the magnetar was reported to have undergone a radio outburst in December, 2018. We observed radio pulsations from XTE J1810–197 during this early phase of its radio revival using the Ultra-Wideband Low receiver system of the Parkes radio telescope, obtaining wideband (704 MHz to 4032 MHz) polarization pulse profiles, single pulses and flux density measurements. Dramatic changes in polarization and rapid variations of the position angle of linear polarization across the main pulse and in time have been observed. The pulse profile exhibits similar structures throughout our three observations (over a week time scale), displaying a small amount of profile evolution in terms of polarization and pulse width across the wideband. We measured a flat radio spectrum across the band with a positive spectral index, in addition to small levels of flux and spectral index variability across our observing span. The observed wideband polarization properties are significantly different compared to those taken after the 2003 outburst, and therefore provide new information about the origin of radio emission.

*Keywords:* pulsar: general – pulsars: individual (XTE J1810–197) – stars: magnetars – stars: neutron.

### 1. INTRODUCTION

Magnetars are a sub-class of pulsars with long rotation periods and high spin-down rates, which regularly undergo X-ray outbursts where the energy released exceeds the spin-down luminosity (see e.g., Kaspi & Beloborodov 2017, for reviews). The anomalous X-ray pulsar (AXP) XTE J1810–197, discovered in early 2003 following an X-ray outburst (Ibrahim et al. 2004), was the first magnetar identified to be a transient pulsating radio source (Camilo et al. 2006). During the early phase of the previous radio outburst, extremely variable flux densities and pulse profiles with

flat spectra were observed (Camilo et al. 2007a,b,c; Kramer et al. 2007; Lazaridis et al. 2008). While different from those of normal radio pulsars, these properties are shared by all four radio magnetars identified so far (Camilo et al. 2007d, 2008; Levin et al. 2010; Keith et al. 2011; Shannon & Johnston 2013), and are similar to those of the high magnetic field pulsar PSR J1119–6127 following its magnetar-like X-ray bursts (Dai et al. 2018). Since the initial detection of its pulsed radio emission, XTE J1810–197 has been regularly monitored by multiple radio telescopes (e.g., Camilo et al. 2016). After rapidly decreasing over the first 10 months, the averaged radio flux density remained steady for the next 22 months before fading and eventually disappearing in late 2008 (Camilo et al. 2016).

For the following 10 years, XTE J1810–197 remained in a quiescent/low-activity state in both radio and X-ray bands (Pintore et al. 2019), until intense radio emission was reported to have restarted sometime between 2018 October 26 and December 8 (Lyne et al. 2018). Follow-up observations have been carried out in radio and X-ray bands by several telescopes, where strong pulsations in both bands have been detected (e.g., Desvignes et al. 2018; Lower et al. 2018; Gotthelf et al. 2018, 2019). Early observations of the outburst and radio revival are of great importance for understanding the origin of magnetar radio emission and to study their behaviour post-outburst. Here we present observations (on 2018 December 11, 15 and 18) of XTE J1810–197, three days after the first report of its revival, using the Ultra-Wideband Low (UWL) receiver system recently installed at the Parkes 64 meter radio telescope (Hobbs et al. 2019). We show wideband polarization pulse profiles, single pulses and flux density measurements of the magnetar during the early phase of its revival, and compare these initial results with previous observations.

## 2. OBSERVATIONS AND DATA REDUCTION

XTE J1810–197 was observed on 2018 December 11, 15 and 18 at Parkes using the UWL receiver, which provides radio frequency coverage from 704 MHz to 4032 MHz. Further observations using the UWL are ongoing and will be the subject of future work. The December 11 observation was performed using the transient search mode where data is recorded with 8-bit sampling every 128  $\mu$ s in each of the 1 MHz wide frequency channels (3328 channels across the whole band). Observations on December 15 and 18 used the pulsar fold mode where data is folded modulo the pulse period with 1024 phase bins in each of the 1 MHz channels, integrated for 30 s and written to disc. For both modes, data were coherently de-dispersed at a dispersion measure (DM) of  $178 \pm 5$  pc cm<sup>-3</sup> (Camilo et al. 2006) with full Stokes information recorded. Total integration times are 819, 1770 and 631 seconds for observations on December 11, 15 and 18, respectively.

At the current stage, a critical sampling filter bank has been used to produce 26 sub-bands. We removed 5 MHz of the bandpass at each edge of the 26 sub-bands to mitigate aliasing. We manually excised data affected by narrow-band and impulsive radio-frequency interference (RFI) for each sub-integration. To measure the differential gains between the signal paths of the two voltage probes, we observed a pulsed noise signal injected into the signal path prior to the first-stage low-noise amplifiers before each observation. The noise signal also provides a reference brightness for each observation. To

correct for the absolute gain of the system, we use observations of the radio galaxy 3C 218 (Hydra A); using on- and off-source pointings to measure the apparent brightness of the noise diode as a function of radio frequency. Polarimetric responses of the UWL are derived from observations of PSR J0437–4715 (Johnston et al. 1993) covering a wide range of parallactic angles (van Straten 2004), taken during the commissioning of UWL in November 2018. The Stokes parameters are in accordance with the astronomical conventions described by van Straten et al. (2010). The linear polarization and the position angle of linear polarization were calculated following Dai et al. (2015). Search-mode data is folded using the DSPSR (van Straten & Bailes 2011) software package. All data reduction and calibration used the PSRCHIVE (Hotan et al. 2004) software package.

## 3. RESULTS

In Fig. 1, we show the total intensity, as well as the linearly and circularly polarized emission and the position angle (PA) of linear polarization, as a function of pulse phase and frequency for data taken on December 11. Across a continuous frequency coverage from 704 MHz to 4032 MHz, pulse profiles show remarkably small frequency evolution. Apart from the leading component and leading edge of the main pulse becoming shallower at higher frequencies and the trailing component disappearing at lower frequencies, the structure, polarization and PA remain similar across the band. We obtain a rotation measure (RM) of  $74.44 \pm 0.16$  rad m<sup>-2</sup>, which agrees with previous measurements (Camilo et al. 2007c). All the PA have been corrected for the measured RM, referred to infinite frequency.

To better present details of polarization pulse profiles, in Fig. 2, we show the average polarization pulse profile of our three observations at four different frequencies. The observed pulse profiles show three components, a wide and shallow leading component, a strong, spiky main pulse and a weak trailing component. The main pulse is similar to that observed after the 2003 outburst, which was found to be dominated by strong, narrow single pulses (Camilo et al. 2007b; Kramer et al. 2007). All three pulse components have high linear polarization across the entire band, consistent with previous observations. The leading and trailing components are almost 100% linearly polarized.

Strong single pulses from XTE J1810–197 were recorded during the search-mode observation on December 11. Individual pulses are found to be comprised of narrow spiky emission components clustered around the phase of the main pulse and scattered throughout the leading and tail components. Similar to multi-frequency

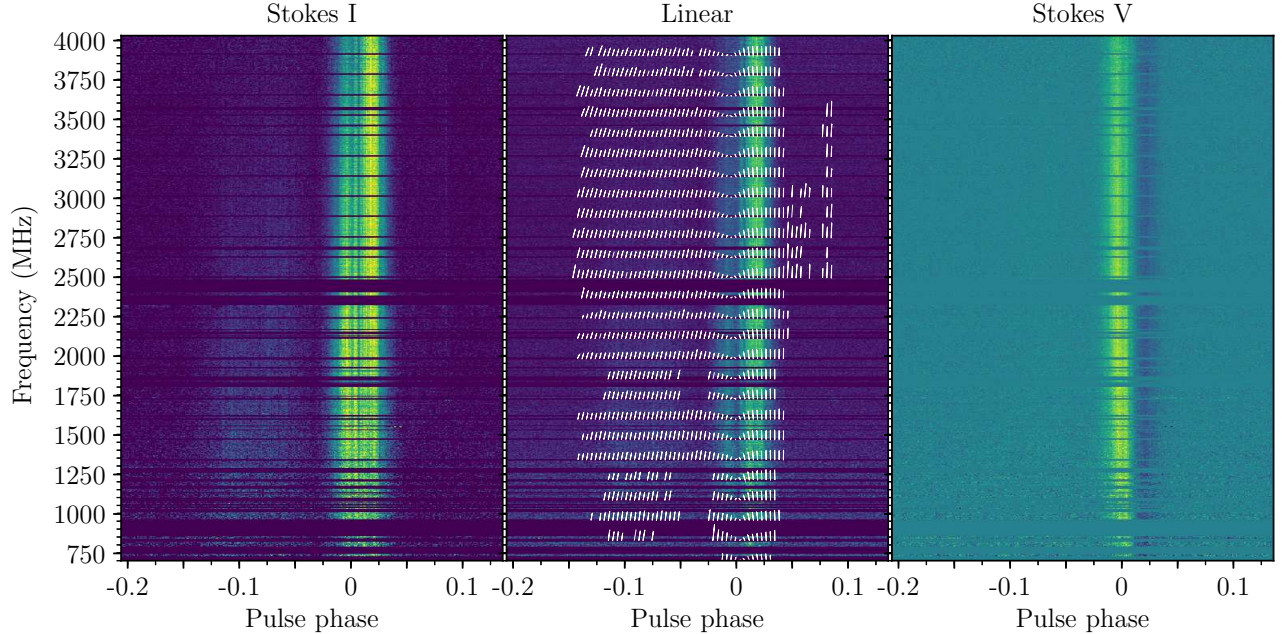


**Figure 1.** Average polarization pulse spectra for XTE J1810–197 taken on 2018 December 11. From left to right, we show Stokes I, linear polarization and Stokes V, normalised by their peak values. Gaps represent zero-weighted channels that were consistently or strongly contaminated by RFI. The PA of the linear polarization (over each 128 MHz subband) is shown as white solid lines. The length of lines represent the fraction of linear polarization.

analyses during the 2003 outburst (Serylak et al. 2009), the amplitudes and number of emission spikes are seen to be highly variable from pulse-to-pulse. A selection of high time resolution, single pulse polarization profiles are presented in Fig. 3. The single emission spikes display remarkable millisecond-width temporal structure and polarization evolution across the pulse cycle. Spikes within the leading, latter part of the main pulse, and tail components are almost completely linearly polarized, whereas those within the leading half of the main pulse show a large degree of circular polarization. The single pulse fluxes remain relatively flat across the UWL band, with little evidence of frequency evolution with phase. We note that single pulses were not recorded for the December 15 and 18 observations. Given the pulse-to-pulse variability seen in this single epoch, the single pulses presented here may not be representative of those in other observations.

An improved estimate of the magnetar’s DM is obtained by generating times of arrival (ToAs) from the high resolution single-pulse archives in Fig. 3. This is achieved by splitting the archives into 64 sub-bands and using the integrated single-pulse profiles as templates. Any residual dispersion in the pulse would result in an increasing delay in the ToAs generated from the high to low frequency sub-bands, which we correct for by fitting the DM using the reduced  $\chi^2$  method implemented in TEMPO2 (Hobbs et al. 2006). From this

method we obtain a mean DM of  $178.51 \pm 0.08 \text{ pc cm}^{-3}$  where the uncertainty is the variance between DM measurements for each pulse. This result represents an improvement over the previous measurement reported in Camilo et al. (2006) by two orders of magnitude. We also obtain a spin-frequency measurement of  $\nu = 0.180463 \pm 0.000007 \text{ Hz}$  from this observation (MJD 58463.963).

To measure the flux density, we formed noise-free standard templates for each observation using the PSRCHIVE program PAAS after integrating the data over the observing band and observation duration. The PSRCHIVE program PSRFLUX was used to measure the flux density for each observation, which cross-correlates the observed profile with the standard template to obtain the scaling factor and then the averaged flux density. The uncertainty of flux density was estimated using the standard deviation of the baseline fluctuations. As described in Section 2, for fold-mode observations, the absolute gain of the system was calibrated using observations of Hydra A. Flux density measurements of the fold-mode observations are listed in Table 1. For current UWL search-mode observations, the absolute gain can not be calibrated. We estimate the search-mode flux density by comparing the baseline root-mean-square (RMS) with that of the calibrated fold-mode observation taken on December 18, which was less affected by RFI.

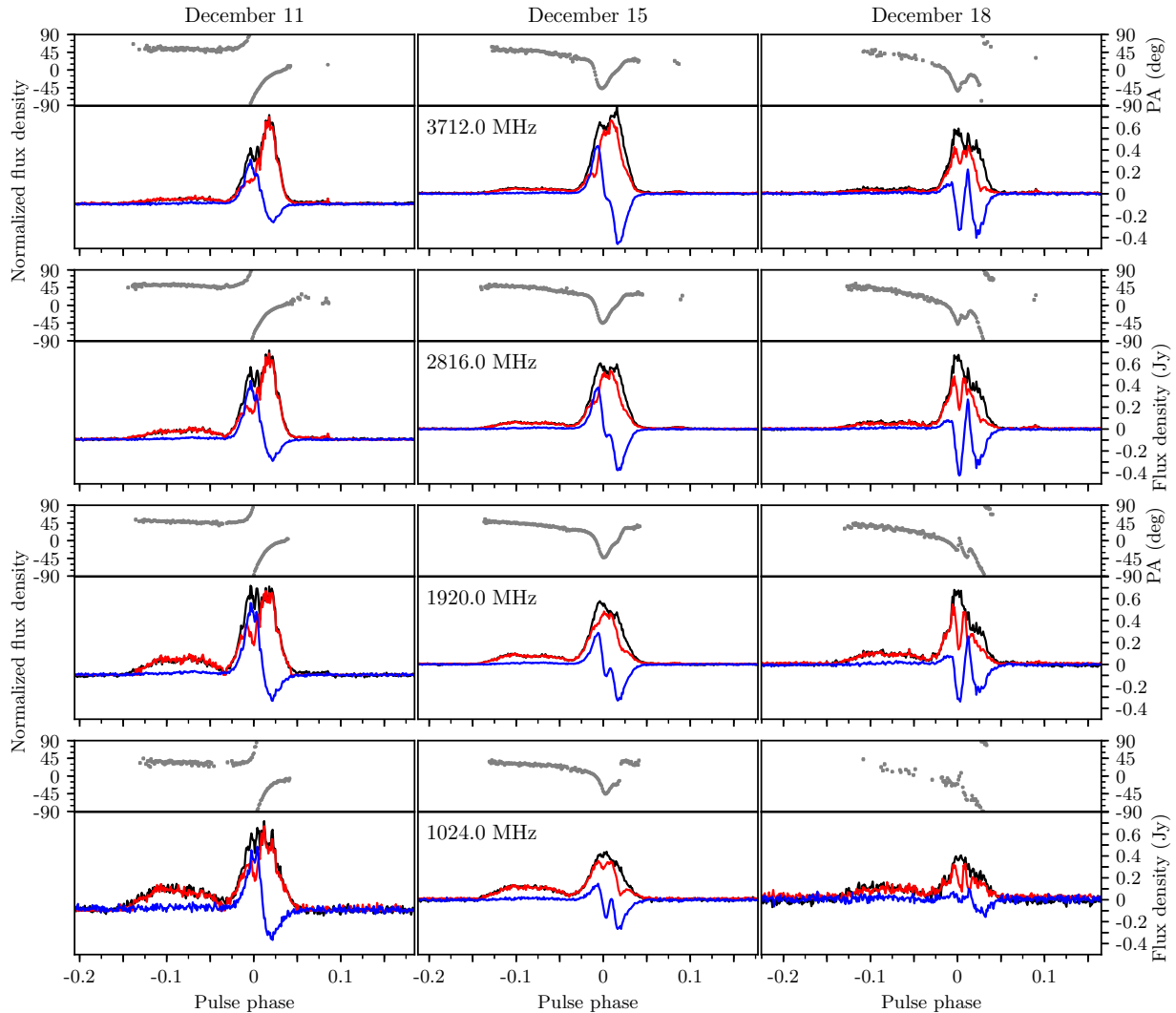


**Figure 2.** Averaged polarization pulse profiles centred at 3712, 2816, 1920 and 1024 MHz (each with a bandwidth of 128 MHz) at three epochs. In each panel, the black line shows total intensity, red linear polarization, and blue circular polarization. The PA of the linear polarization is shown in the top panels. Search-mode observation on December 11 is not flux calibrated, and therefore we show the normalized flux density.

With the UWL, we were able to simultaneously measure flux densities across a wideband and mitigate the effect of large flux density variations. In Fig. 4, we show flux density measurements of our three observations. Large variations in search-mode observation flux densities are likely to be introduced by low level RFI in the baseline. Although the spectral shape shows significant variations, the spectra generally follow a power-law with positive spectral indices. Fitting a power law spectrum of the form  $S_\nu \approx \nu^\alpha$  to measurements on December 15, we measure a spectral index of  $\alpha \approx +0.3$ .

#### 4. DISCUSSION

Our observations captured the wideband polarization properties of the magnetar during the early stages of its latest outburst. We observed several differences in the pulse profile properties when compared to those observed after the 2003 outburst (Camilo et al. 2007b,c; Kramer et al. 2007). Firstly, the overall structure of the pulse profile did not show dramatic changes during our observations over a week period, with the leading and trailing components remaining stable. Secondly, we observed strong circular polarization in the main pulse and no evidence of an interpulse. However, the highly linearly polarized leading component with flat and stable PA swing is reminiscent of the previously observed inter-



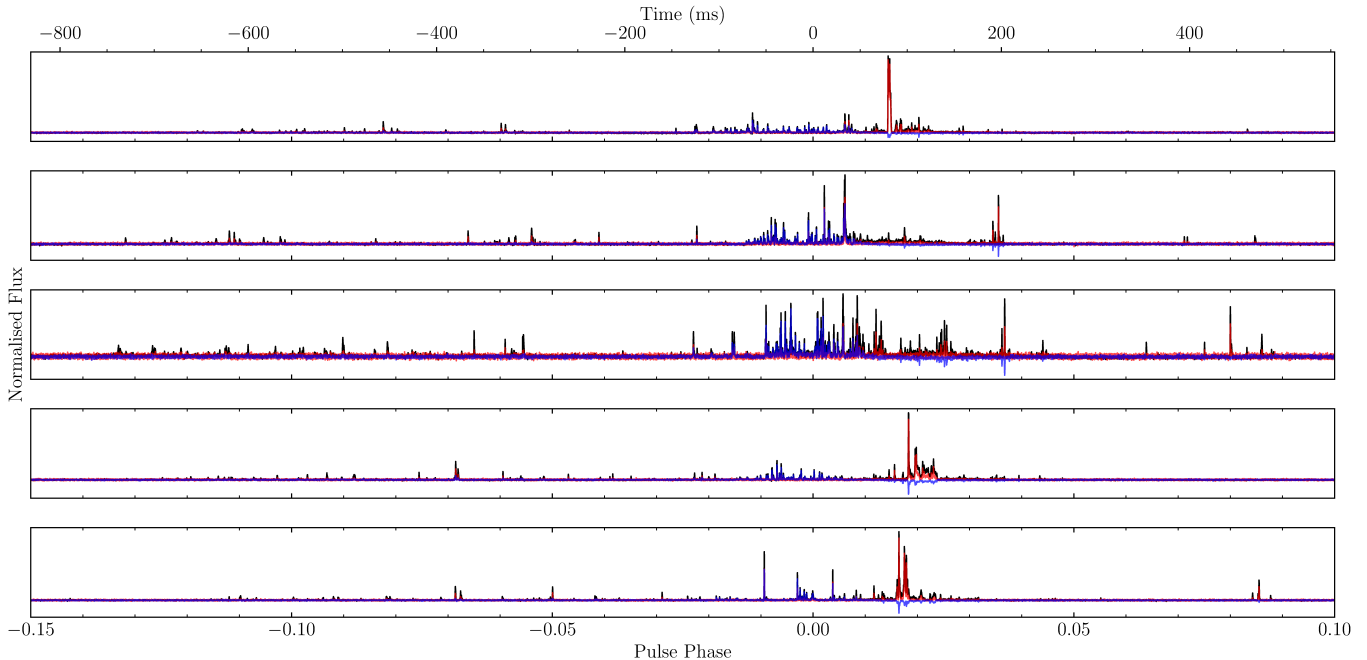


**Figure 3.** A selection of high time resolution polarimetric single pulse profiles seen on December 11th, 2018. The integrated profiles show the total intensity in black, linear polarization in red and circular polarization in blue.

pulse. Finally, unlike the relatively stable polarization properties of the main pulse reported by Camilo et al. (2007c) and Kramer et al. (2007), we observed significant changes in both the linear and circular polarization across the main pulse. The PA swing across the main pulse changed in both shape and absolute value over a week period, and show complex structures which deviate from a simple rotating vector model (RVM, Radhakrishnan & Cooke 1969). Interestingly, the PA

**Table 1.** UWL measurements of period-averaged flux densities.

Flux Density (mJy)	December 15	December 18
$S_{768}$	$18.8 \pm 0.3$	$14.2 \pm 0.4$
$S_{1024}$	$22.6 \pm 0.2$	$20.3 \pm 0.2$
$S_{1280}$	$25.2 \pm 0.2$	$23.9 \pm 0.2$
$S_{1536}$	$26.8 \pm 0.1$	$27.1 \pm 0.1$
$S_{1792}$	$28.9 \pm 0.1$	$29.6 \pm 0.1$
$S_{2048}$	$29.3 \pm 0.1$	$30.7 \pm 0.1$
$S_{2304}$	$30.05 \pm 0.08$	$30.9 \pm 0.1$
$S_{2560}$	$31.11 \pm 0.05$	$30.31 \pm 0.09$
$S_{2816}$	$31.64 \pm 0.05$	$30.36 \pm 0.09$
$S_{3072}$	$33.18 \pm 0.07$	$28.91 \pm 0.09$
$S_{3328}$	$34.2 \pm 0.1$	$29.7 \pm 0.1$
$S_{3584}$	$36.4 \pm 0.1$	$28.3 \pm 0.1$
$S_{3840}$	$35.7 \pm 0.2$	$29.9 \pm 0.2$

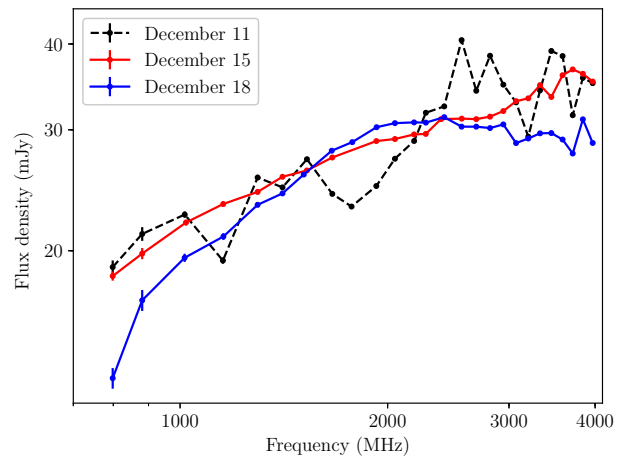


**Figure 4.** Flux density as a function of frequency. For the search-mode observation taken on 2018 December 11 (black points with dashed lines), flux densities were calibrated as described in Section 3. Red and blue points with solid connecting lines represent the flux density measured during fold-mode observations on December 15 and 18.

of the leading and trailing components show almost no variation in time at all.

When compared to observations after the previous outburst, the difference in polarization properties we observe might indicate structural changes in the magnetosphere triggered by the latest outburst, with the possibility that we are observing radio emission from a

new active region. Changes in the PA swing were also observed in PSR J1622–4950 after its recent radio activation in 2017, which can generally be modelled by a RVM with variations explained by different emission locations within the magnetosphere (Levin et al. 2012; Camilo et al. 2018). However, the observed PA swing of XTE J1810–197 shows complex structures and does not follow the RVM model obtained during the previous outburst (Camilo et al. 2007c). In addition, by comparing the radio and X-ray profiles, Gotthelf et al. (2019) show that the macroscopic geometry of the magnetic field associated with the emission did not change between outbursts.

Alternatively, it has been suggested that magnetospheres of magnetars can become twisted by sudden crustal motion, where the untwisting of magnetic field lines dissipates magnetic energy and produces electromagnetic radiation (e.g., Beloborodov 2009). In this scenario, radio emission may originate on the bundle of closed field lines, and large variations in polarization properties can be explained by the instabilities in the twisted magnetosphere. While the polarization and PA were observed to change on a time scale of days, we note the overall shape of total intensity remained relatively similar, including the profile width and separation between different components.

Furthermore, we observe little frequency evolution in the pulse profile and polarization properties over our wide band. Camilo et al. (2007c) compared the pulse profile during the previous outburst at 1.4, 3.2 and 8.4 GHz, showing the double-peaked profile became narrower at higher frequencies, and the ratio of the leading to trailing component becomes larger. Here we also observe the ratio of the leading to main component becomes larger, but find no evidence of profile narrowing at higher frequencies. The lack of profile and polarization evolution over such a wide band puts tight constraints on current models of the origin of radio emission from magnetars. For the twisted magnetosphere model, twists of magnetic fields are expected to be larger as one goes further along a given field line, which would result in observable differences in the polarization profile as a function of frequency.

For XTE J1810–197, significant variation of PA swing and absolute PA values have only been observed for the interpulse after the 2003 outburst (Kramer et al. 2007), which is argued to be evidence of magnetospheric propagation effects in a non-dipolar magnetic field configuration. Such propagation effects might also explain the origin of circular polarization not observed before. If the PA swing variations are caused by magnetospheric propagation effects, the three adjacent pulse components we

observe must originate from very different locations in the magnetosphere and the dramatic variation we observed implies very strong propagation effects at the early stage of the outburst.

A similar example of dramatic changes in polarization within a short period of time was observed in the high magnetic field pulsar J1119–6127 after a magnetar-like X-ray burst. The dramatic profile and PA variations of PSR J1119–6129 was accompanied by peculiar spin-frequency evolution and large fluctuation of flux density, which have been suggested to be linked with either reconfiguration of magnetic field or strong particle winds (Dai et al. 2018). Similar changes in the magnetosphere could also be triggered by the outburst of XTE J1810–197, and produced the observed polarization variation.

The radio spectrum of XTE J1810–197 after the 2003 outburst was studied by Camilo et al. (2007a); Lazaridis et al. (2008), where a spectral index of  $-0.5 \lesssim \alpha \lesssim 0$  over the range of 1.4 to 144 GHz was observed. We observed a harder spectrum than what was measured after the 2003 outburst. The spectrum shape showed changes with time over the ten day observing span, but we find no evidence of the dramatic variations in  $\alpha$  that have previously been observed in XTE J1810–197 (e.g., Lazaridis et al. 2008) and other radio magnetars (Camilo et al. 2008; Levin et al. 2010; Pennucci et al. 2015). On December 18, we observe evidence of a spectral turnover at around 2 GHz.

At 1.4 GHz, we measured an average flux density of  $\sim 20$  mJy at all three epochs, which is about a factor of two higher than those measured at the first detection of radio pulsations from XTE J1810–197 (Camilo et al. 2006). Observations beginning three years after the 2003 outburst showed that the flux density decreased by a factor of 20 during 10 months in 2006. Similarly, measurements of the magnetar PSR J1622–4950 soon after its radio revival in early 2017 reached a maximum averaged flux density of tens of mJy at 1.4 to 3 GHz (Camilo et al. 2018). These suggest that the wide band observations presented here might be during the most radio-active period of the current outburst.

## 5. SUMMARY

After 10 years in a radio silent state, pulsed radio emission from the magnetar XTE J1810–197 was found to have reactivated in early December 2018. We conducted follow-up observations using the UWL receiver of the Parkes telescope on 2018 December 11, 15 and 18. Ultra-wideband polarization pulse profiles, single pulses and flux density measurements during the early phase of the outburst are presented in this paper. While pulse

profiles of the total intensity show similar structures during the three epochs, the polarization properties show significant variability. We also find the PA swing varied dramatically across the main pulse and in time, however it remained stable across the leading and trailing pulse components. Despite dramatic variations in time, very little frequency evolution of the polarization have been observed across the wideband. Compared with measurements after the previous outburst, we find the flux density of XTE J1810–197 to be at least a factor of two higher, which could be due to our observations capturing an earlier stage of the radio outburst. Radio spectra across the wideband generally follow a power-law with positive spectral indices, and show small levels of variation across the observation epochs. The wideband polarization properties are quite different to what was seen during the previous outburst and showed dramatic variations in time, which might indicate rapid changes

in the magnetosphere soon after the outburst. Future multi-wavelength, long term monitoring of this pulsar is required to complete the full picture of the magnetar outburst behaviour.

We thank the Parkes team for their great efforts during the installation and commissioning of the UWL receiver system. We thank Maxim Lyutikov for useful discussions. The Parkes radio telescope is part of the Australia Telescope National Facility which is funded by the Commonwealth of Australia for operation as a National Facility managed by CSIRO. Part of this work made use of the OzSTAR national HPC facility. Work at NRL is supported by NASA. We also acknowledge use of the Astronomer’s Telegram and the NASA Astrophysics Data Service.

## REFERENCES

- Beloborodov, A. M. 2009, *ApJ*, 703, 1044
- Bernardini, F., Perna, R., Gotthelf, E. V., et al. 2011, *MNRAS*, 418, 638
- Camilo, F., Ransom, S. M., Halpern, J. P., et al. 2006, *Nature*, 442, 892
- Camilo, F., Ransom, S. M., Peñalver, J., et al. 2007a, *ApJ*, 669, 561
- Camilo, F., Cognard, I., Ransom, S. M., et al. 2007b, *ApJ*, 663, 497
- Camilo, F., Reynolds, J., Johnston, S., et al. 2007c, *ApJL*, 659, L37
- Camilo, F., Ransom, S. M., Halpern, J. P., & Reynolds, J. 2007d, *ApJL*, 666, L93
- Camilo, F., Reynolds, J., Johnston, S., Halpern, J. P., & Ransom, S. M. 2008, *ApJ*, 679, 681
- Camilo, F., Ransom, S. M., Halpern, J. P., et al. 2016, *ApJ*, 820, 110
- Camilo, F., Scholz, P., Serylak, M., et al. 2018, *ApJ*, 856, 180
- Dai, S., Hobbs, G., Manchester, R. N., et al. 2015, *MNRAS*, 449, 3223
- Dai, S., Johnston, S., Weltevrede, P., et al. 2018, *MNRAS*, 480, 3584
- Desvignes, G., Eatough, R., Kramer, M., et al. 2018, *The Astronomer’s Telegram*, 12285
- Gotthelf, E. V., Halpern, J. P., Grefenstette, B.W., et al. 2018, *The Astronomer’s Telegram*, 12297
- Gotthelf, E. V., Halpern, J. P., Alford J. A. J., et al. 2019, *ApJ*, submitted, arXiv:1902.08358.
- Hobbs, G., et al. 2019, in preparation.
- Hobbs, G. B., Edwards, R. T., & Manchester, R. N. 2006, *MNRAS*, 369, 655
- Hotan, A. W., van Straten, W., & Manchester, R. N. 2004, *PASA*, 21, 302
- Ibrahim, A. I., Markwardt, C. B., Swank, J. H., et al. 2004, *ApJL*, 609, L21
- Johnston, S., Lorimer, D. R., Harrison, P. A., et al. 1993, *Nature*, 361, 613
- Kaspi, V. M., & Beloborodov, A. M. 2017, *ARA&A*, 55, 261
- Keith, M. J., Johnston, S., Levin, L., & Bailes, M. 2011, *MNRAS*, 416, 346
- Kramer, M., Stappers, B. W., Jessner, A., Lyne, A. G., & Jordan, C. A. 2007, *MNRAS*, 377, 107
- Lazaridis, K., Jessner, A., Kramer, M., et al. 2008, *MNRAS*, 390, 839
- Levin, L., Bailes, M., Bates, S., et al. 2010, *ApJL*, 721, L33
- Levin, L., Bailes, M., Bates, S. D., et al. 2012, *MNRAS*, 422, 2489
- Lower, M. E., Bailes, M., Jameson, A., et al. 2018, *The Astronomer’s Telegram*, 12288
- Lyne, A., Levin, L., Stappers, B., et al. 2018, *The Astronomer’s Telegram*, 12284
- Pennucci, T. T., Possenti, A., Esposito, P., et al. 2015, *ApJ*, 808, 81
- Pintore, F., Mereghetti, S., Esposito, P., et al. 2019, *MNRAS*, 483, 3832
- Radhakrishnan, V., & Cooke, D. J. 1969, *Astrophys. Lett.*, 3, 225
- Serylak, M., Stappers, B. W., Weltevrede, P., et al. 2009, *MNRAS*, 394, 295

Shannon, R. M., & Johnston, S. 2013, MNRAS, 435, L29

van Straten, W. 2004, ApJS, 152, 129

van Straten, W., Manchester, R. N., Johnston, S., &  
Reynolds, J. E. 2010, PASA, 27, 104

van Straten, W., & Bailes, M. 2011, PASA, 28, 1